Simulation and Experimental Analysis of Hovering and Flight of a Quadrotor

Weerasinghe S.R.* and Monasor M.
*Author for correspondence
Department of Engineering Design and Mathematics
Faculty of Environment and Technology
University of the West of England
Coldharbour Lane, Frenchay, Bristol BS16 1QY,
United Kingdom,
E-mail: rohitha.weerasinghe@uwe.ac.uk

ABSTRACT

Quadcopters were the first heavier than air vertical take-off landing vehicles. Quadrotors have become increasingly popular in the recent years finding a great variety of applications in different fields such as surveillance and small goods transport. The flight of quad-rotors are not easily analysed, but computational fluid dynamic simulations are a credible source of reliable modelling. In the present paper, an analysis in computational fluid dynamics (CFD) is presented performed on a quadrotor model SYMA X5SC with focus on the fuselage and the rotor blades.

The quadrotor is analysed in three different models; fuselage, rotor and full configuration. The models have been designed using CAD tools and encapsulated in a volume domain. Volume unstructured meshes are used and contain a maximum of 3.5 million of cells. Each blade was assigned to a moving cell zone making it possible to rotate. Steady and unsteady flow simulations have been carried out. Hover, and forward and side wind cases were inspected. The flight was simulated for the hovering mode at three different angles of attack and free stream velocities.

Wind tunnel experimentation of the quadrotor flow field was carried out to obtain experimental data to compare against CFD results. Optimised CFD results are in good agreement with the measurements and are presented in comparison with the simulation results.

This study presents an analysis of the quadrotor flow and highlights the main aerodynamic features. The flow analysis allows accurate prediction of aerodynamic loads on a quadrotor in various flight conditions.

NOMENCLATURE

AoA	[°]	Angle of Attack
Special characters		
Ω	[rad/s]	Angular velocity
ω	[/s]	frequency
$\boldsymbol{k}$	[m^2/s^2]	Turbulent kinetic energy
ε	[m^2/s^2]	Turbulent kinetic energy dissipation
$\boldsymbol{u}$	[m/s]	Absolute velocity
$\boldsymbol{v}$	[m/s]	Whirl velocity
ν	[m/s^2]	Eddy viscosity
x	[m]	Cartesian axis direction
ρ	[kg/m^3]	Density
μ	[kg/sm]	Molecular viscosity
$\frac{\partial}{\partial x}$	[]	Partial derivative (with respect to x)
Subscripts		
max		Maximum
min		Minimum

INTRODUCTION

In recent years, quadrotors have been studied both in civil and military applications becoming progressively more popular. Due to its specific capabilities, use of autonomous quadrotor vehicles has been envisage for a variety of applications; both as individual vehicles and in multiple vehicle teams, including surveillance, search and rescue and mobile sensor networks (Hoffmann, Waslander and Tomlin, 2006). The use of quadrotors can minimize the human risks in hazardous environments and contribute to faster and more effective disaster relief operations.

Quadrotors are chosen in many applications because of their basic structure, their ability to move in every direction and to perform better than helicopters in hover. Also, unlike helicopters, quadrotors cannot change their blade's angle of attack (A.o.A.), making them mechanically simpler. However, some negative aspects can be pointed out too; like the high energy consumption, the low lifting capacity, or the loss of altitude and attitude control at certain wind speed on free environments or during aggressive manoeuvring. It is important to make some developments so that the quadrotors can be used with high reliability in most situations.

Computational Fluid Dynamics (CFD) is a powerful tool used as a prediction instrument in aerodynamics applications. Many studies have focused in the study of helicopter aerodynamics in the past two decades with successful results, proving the usefulness of CFD for rotor based models. However, quadrotors are quite new to this line of studies making it challenging, generally due t the geometrical complexity and the need to handle the motion of the four propellers relative to the fuselage.

In this paper, one of the most common quadrotors, the Syma X5SC has been selected to subject to CFD analysis in order to define the forces and describe the aerodynamic features

surrounding it. The simulations included several flow and flight configurations, involving different angles of attack and incoming wind speeds. CFD simulations of the full quadrotor (fuselage + rotors) will fully describe the physical phenomena arising from the quadrotor flight. Additionally, simulations of the fuselage and a single rotor were carried out to analyse these parts separately. Wind tunnel testing were performed to generate experimental data for validation of results of the CFD simulations.

Forces acting on the quadrotor were measured in wind tunnel tests and the data obtained is used to compare the accuracy of the simulations. A good quality mesh and the selection of the most appropriate turbulence model are an important part of this study. Steady and unsteady simulations are taken in count to find the best method to describe the quadrotor functioning in good relation with the computational time.

With the availability of CFD some attempts have been made by a number of people in explaining the rotodynamics of a flying objects, especially helicopters. Some of the early investigations were done by Marcel, Massimo and Giovanni. Steigi and Barakos have done significant work on CFD analysis of helicopter aerodynamics. Xu and Ye have performed investigations on rotor and frame interaction using CFD.

QUADCOPTER CONTROLS AND AERODYNAMICS

A quadrotor is an unmanned aerial vehicle (UAV) formed by a cross structure with four rotors situated at the arm edges. The electronic systems, the battery and the possible additional load carried by the quadrotor are placed in the central structure. The lift force necessary to elevate the model from the ground and maintain the body in flight is achieved through the force generated by the four rotors, for what the addition of all forces must be, higher than the weight.

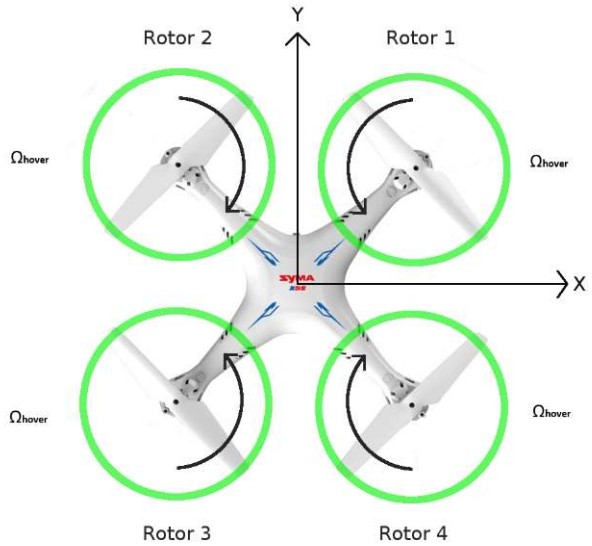

Figure 1: Hover flight configuration

There are four quadrotor basic flight operations:

Hover flight: maintains a constant altitude. To accomplish this, all rotors rotate at the same angular velocity (hover velocity) to produce the same lift (Figure 1). The sum of lift forces must be equal to the weight generated by the quadrotor.

Axial flight: is provided by all rotors moving at the same angular velocity. The quadcopter will ascend or descend depending on whether the rotation velocity is higher or lower than the hover velocity, respectively.

Yaw:, the rotation around the z axis in positive direction is achieved by applying an increment in the angular velocity of rotors 1 and 3, and a decrease of the same magnitude on the angular velocity or rotors 2 and 4 (Fig2). For a negative rotation around the z axis the increment is applied to the rotors 2 and 4, and the decrease to the 1 and 3. This way, the rotation is completed maintaining the lift force and hence maintaining hover flight.

Forward flight: is executed in two directions, in x and y axis. From hover flight, forward flight can be achieved by applying an angular velocity increment to the rotors 1 and 2, and a decrease of the same magnitude on the angular velocity of the rotors 3 and 4 . This way, the quadrotors would start moving in negative y direction. Similar functioning happens to forward flight in x direction.

Aerodynamic effects

Extensive literature (Leishman, 2006) (Seddon and Newman, 2011) is found in mechanics of helicopter aerodynamics. These aerodynamic effects can be easily applied to quadrotors. However, quadrotors present some peculiar aerodynamic effects that are discussed in this section. These effects can be ignored at slow velocities, for example while hovering or during forward flight under 3 m/s (Huang, Hoffman, Waslander and Tomlin, 2009). Nevertheless, even at moderate velocities, the impact of the aerodynamic effects resulting from variation in air speed can be significant.

Total thrust variation in transitional horizontal flight that result in two effects: the expected lift generated by the rotors and a change in thrust due to the angle of attack. As the rotors move horizontally, an increase in lift is caused by the relative momentum of the airstream (Huang, Hoffman, Waslander and Tomlin, 2009). This is known as translational lift. The angle of attack of the rotors with respect to the free stream also changes the lift. An increase in the angle of attack increases thrust (Leishman, 2006).

Interference caused by the parts of the model close the rotor stream: Components near the rotor stream cause unsteady thrust behaviour and poor attitude control, and this interference has been proved to be considerably influenced by airframe modifications (Hoffman 2006).

These aerodynamic effects were studied, analysed through wind tunnel testing and CFD simulations, and results presented in this paper.

EXPERIMENTAL ANALYSIS -WIND TUNNEL TESTING

A wind tunnel is one of the most common experimental testing facilities for testing of fluid flows (Pope, 1966). The quality of the results obtained in a wind tunnel depends on the quality of

the free-stream flow. Achieving a good quality free-stream flow is of great importance for studies of external flows with separated shear layers, we can include here a flow separation on a wing or a turbulent wake on a bluff (Mehta and Bradshaw, 1979). In this study, quadrotor under study was wind tunnel tested. The experimental data are used for the validation of the CFD simulations. Several flow configurations were considered in order to simulate a free air environment.

A subsonic wind tunnel was used for the testing with a maximum wind speed of 50 m/s, and a high speed working section dimensions of 2.44 m x 2.14 x 1.59 m.

The prototype used for testing was the Syma X5CS quadrotor (1:1 scale) mounted on a wooden support with a metallic attachment. This support was connected to the mounting structure through a metal bar and to a couple of wires to balance the angle of attack. The support was designed to avoid ground effect and to have the smallest possible influence on the rotor flow. The set up was carefully planned to avoid any obstructions, such as balance or walls closer than 1.5 rotor diameters.

Figure 2: Wind tunnel set up (fuselage and rotors).

Four different set ups were tested following the configuration of the CFD simulations. First, the support was tested on its own for later calculation of the added values. Secondly, the fuselage was tested. After that, the full quadrotor, combination of rotors, and fuselage were tested in two runs: a first one with no induced angular velocity on the rotors, and a second one supplying the power associated to the angular velocity necessary to establish a hover flight on free stream. The quadrotor has a mass of 96 grams, so it has to compensate a weight of 0.94N for that flight condition.

Drag and lift forces were measured for a substantial number of test cases that are combinations of various rotor speed, angles of attack and free stream velocities. A first run without the model was taken to stablish the zero configuration. After that, four different free stream velocities between 0 and 15 m/s were scanned at two different angles of attack, 0° and -10°. Although the input power was maintained through the different cases, the angular velocity resulted different for each wind tunnel speed. Table 1 and Table 2. Show a summary of the different test configurations.

All forces measured without the rotors give the loads acting on the body. These values were deducted from the values measured with the rotors to find the total rotor lift and drag forces. Similarly, the values obtained for the support were subtracted from the fuselage values to obtain the fuselage net forces.

The main results of the wind tunnel experimentation carried out with the Syma X5SC model in all its configurations are outlined in the present section. The tests performed with a wind tunnel velocity of 0 m/s and 10 m/s were repeated twice. The tests carried out for 5 m/s and 15 m/s wind tunnel speed were run only once. In the hover simulation, the angular velocities obtained were of 4.220 r.p.m., 4.080 r.p.m. and 3.900 r.p.m for 0 m/s, 5 m/s and 10m/s respectively. In the case of 15 m/s it was not possible to obtain this value for the 15 m/s cases due protocol measures, so a progressive estimation of 3.760 r.p.m. was considered.

Table 1 Wind tunnel results at 0 °

0° A.O.A.	WIND TUNNEL SPEED							
MODEL CONF.	0 m/s		5 m/s		10 m/s		15 m/s	
	Lift	Drag	Lift	Drag	Lift	Drag	Lift	Drag
Fuselage	X	X	0.14	0.1	0.1	0.35	-0.04	0.71
Fuselage + rotors (power off)	X	X	0.18	0.18	0.18	0.48	0.43	0.89
Fuselage + rotors (power on)	0.96	0.00	1.12	0.25	1.3	0.50	1.75	1.14
Rotor (power on)	0.24	0.00	0.24	0.04	0.31	0.04	0.33	0.1

Table 2 Wind tunnel results at 10 °

-10° A.O.A.	WIND TUNNEL SPEED							
MODEL CONF.	0 m/s		5 m/s		10 m/s		15 m/s	
	Lift	Drag	Lift	Drag	Lift	Drag	Lift	Drag
Fuselage	X	X	0.1	0.12	0.35	0.3	0.4	0.7
Fuselage + rotors								
(power off)	X	X	0.77	0.25	0.7	0.59	0.78	0.98
Fuselage + rotors (power on)	0.93	0	1.21	0.25	1.42	0.51	1.79	0.95

No correction was needed for the wind tunnel data due to the use of a 1:1 scale model. Table 2 and Table 3 present the results for the before mentioned calculations to obtain the net forces for both the rotors and the fuselage. These values calculated from

the experimental data can be used to check the quality of the CFD simulations. The data directly extracted from the wind tunnel for the first and the second test can be found on the Appendix.

The data obtained for the rotors revolution shows the first signs of how the lift generated increase with the wind tunnel speed in line with the transitional lift aerodynamic effect. At the same time, it can be appreciated how the decrease in the angle of attack from 0° to -10° caused a decrease on the lift generated by the rotors movement. High lift values obtained for the full quadrotor model with no induced power at -10° of angle of attack show the complex aerodynamics between the fuselage and the rotor on this configuration.

COMPUTATIONAL MODELLING

Numerical modelling of the physical phenomena observed in experimental analysis is achieved through a computational fluid dynamic (CFD) analysis. Representation of correct physical phenomena and a quality mesh representation is of high importance.

Governing Equations

Use of CFD in the simulations lead to describe the flow field using the governing equations. A sliding mesh simulation has also been used in the study. Numerous studies are available, especially in helicopter aerodynamics how the flowfield is numerically represented in CFD. Steijl and Barakol describe in depth how sliding mesh algorithms can be used in CFD to describe helicopter rotor-fuselage aerodynamics.

Steady state Reynolds-averaged Navier-Stokes equations are used in representing the flow field. The conservation of mass is given as;

$$\frac{\partial}{\partial x_i}\left(\rho u_i\right) = 0 \tag{1}$$

and the conservation of momentum is written as:

$$\frac{\partial}{\partial x_i}\left(\rho u_i u_j\right) = -\frac{\partial p}{\partial x_i} + \frac{\partial}{\partial x_j}\left[\mu\left(\frac{\partial u_i}{\partial x_j} + \frac{\partial u_j}{\partial x_i} - \frac{2}{3}\delta_{ij}\frac{\partial u_k}{\partial x_k}\right)\right] + \frac{\partial}{\partial x_j}\left(-\rho\overline{u_i' u_j'}\right) \tag{2}$$

The Reynolds stress above must be modelled and it can be achieved via a Boussinesq hypothesis.

$$-\rho\overline{u_i' u_j'} = \mu_t\left(\frac{\partial u_i}{\partial x_j} + \frac{\partial u_j}{\partial x_i}\right) - \frac{2}{3}\left(\rho k + \mu_t\frac{\partial u_k}{\partial x_k}\right)\delta_{ij} \tag{3}$$

Here, is the turbulent viscosity and is the turbulent kinetic energy. A turbulence model has to be employed to close this where the SST (shear stress transport) model has been used in this work.

SST model is a $k-\omega$ based turbulence model where the model combines Wilcox and $k-\varepsilon$ model. The transport behaviour is obtained through a limiter to the formulation of eddy-viscosity:

$$\nu_t = \frac{a_1 k}{\max(a_1\omega, SF_2)} \quad \text{, where} \tag{4}$$

$$\nu_t = \frac{\mu_t}{\rho} \tag{5}$$

F_2 is a blending function which restricts the limiter to the wall boundary layer, as the underlying assumptions are not correct for free shear flows. S is an invariant measure of the strain rate. The production term of turbulence frequency ω is given by:

$$P_\omega = \left(\frac{\alpha_3}{\nu_t}\right)P_k \tag{6}$$

Where α_3 is a chosen constant. P refer to production terms.

A rotating reference frame is employed here to render a problem, i.e. which is unsteady in the stationary (inertial) frame steady with respect to the rotating frame. For a steadily rotating frame (i.e., the rotational speed is constant), it is possible to transform the equations of fluid motion to the rotating frame such that steady state solutions are possible.

For a co-ordinate system that rotates steadily with angular velocity Ω relative to a stationary reference frame, the fluid velocities can be transformed from a stationary frame to a rotating frame as

$$\boldsymbol{u}_r = \boldsymbol{u} - \boldsymbol{v}_r \text{, where} \tag{7}$$

$$\boldsymbol{v}_r = \Omega \times \boldsymbol{r} \tag{8}$$

Governing equations for fluid flow for a steadily rotating frame by the relative velocity formulation can be obtained with the above equation (7) and (8).

Computational Model Set up

The fuselage model was comprised of complex shapes and curves. With physical measurements, the fuselage CAD model in Figure 3 was finished with certain facility once the dimensions were established.

Figure 3 - Fuselage CAD model

The rotor model resulted more complicated to produce. The rotors mounted on the SYMA X5SC are particularly thin and

with a changing section from the centre to the tip. The complicated geometry of these rotors causes problem in generating a CAD model, and also for the generating a good quality mesh. The propeller dimensions were carefully measured at several sections and a representative CAD model was developed. In order to simplify the rotor CAD model, the hub was not included on its design.

From a meshing perspective, the CAD model poses two problems: definition errors and representation problems. Definition errors involve geometric and topological errors in the model, such as inverted faces, gaps between surfaces, faces with negative areas, overlapping faces, etc. Simplifying the model means to detect and remove details that are not relevant to the analysis or have a marginal impact on the calculations and make the mesh generation difficult (White, Saigal and Owen, 2003).

The rotor model is composed of a small number of features and it does not allow many simplifications on its geometry. The rotors geometry is critical for a good quality mesh. Sharp edges and narrow passages should be avoided on a good mesh generation, but in the case of the rotors the simplification of those features was discarded as it would change the actual nature of the rotors. However, an important change was introduced when the centre of the rotor was substituted by a cylinder connecting both sides of the propellers to ease the mesh generation (Fig. 3).

Mesh

The quality of the mesh plays an important role on the simulations. A low quality mesh may cause numerical problems, increasing the possibility of divergence and poor results. Existence of complex geometries and the creation of inflation layers compromise quality of the meshes. In order to obtain a balance between keeping a representative geometry whilst keeping a quality mesh, the quality of the elements conforming the meshes was checked with the aspect ratio and skewness quality standards. A mesh can be considered satisfactory when the minimum aspect ratio on the domain is higher than 0.01 and the maximum skewness is lower than 0.98.

Table 3 - Mesh statistics

Mesh	*Orthogonal Quality*		*Skewness Quality*		*Nodes*	*Elements*
	Min.	Ave.	Max.	Ave.		
Fuselage	0.039	0.87	0.89	0.23	749.201	1.957.982
Rotor	0.036	0.82	0.96	0.27	299.184	1.029.095
Full Quadrotor	0.016	0.84	0.96	0.25	1.126.122	3.182.630

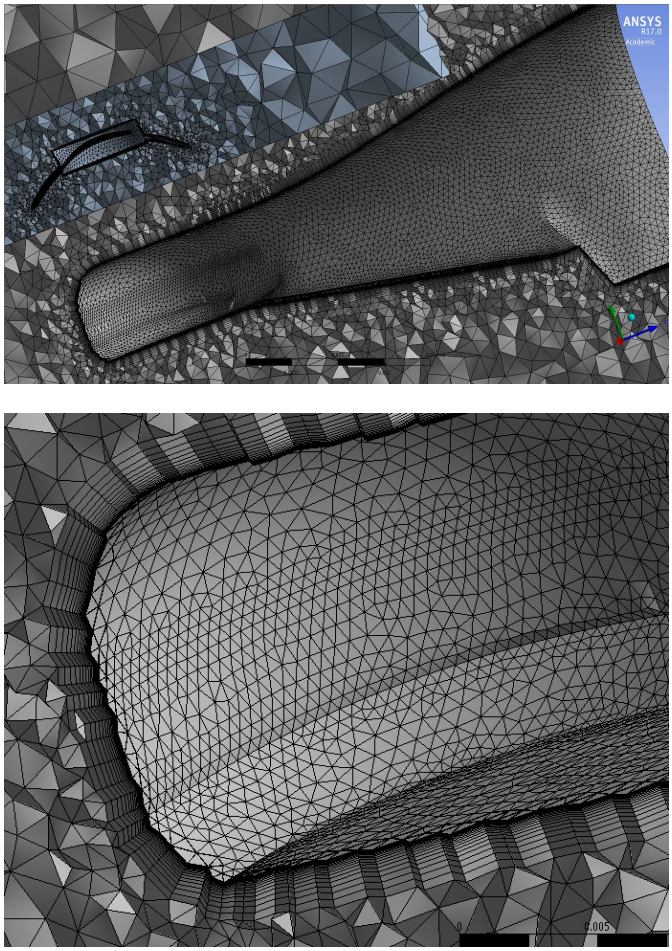

Figure 4; Fuselage Inflation layer

SIMULATIONS

The full quadrotor and the two stripped versions were studied under several flow configurations. Following the wind tunnel experimentation, the models were analysed at 0 m/s, 5 m/s, 10 m/s and 15 m/s wind speed for two angles of attack of 0° and -10°. Having in count these speeds and the quadrotor geometries, the Reynolds number is high enough to consider a fully turbulent flow. In this cases the Mach number is bellow one, so the compressibility effects can be ignored. For this reason, the analysis was established as incompressible.

Initially, short simulations were taken in count to check the residuals convergence and this way guarantee the good functioning of the meshes. Faster the residuals diminish, higher the convergence is, and lower the values are, more accurate the results will be. These simulations were run in steady state and comprised from 50 to 100 iterations. Problems were found in some meshes, always involving the rotors area. These meshes were sent back to ANSYS Meshing for further improvement. Once the residuals found convergence, several volume density controls were introduced to refine the grids. These refinements, like the ones shown in Fig. 26, are useful to obtain a higher precision on critical areas where high pressure gradients were

found. This method allows a better definition of important flow features, such as wakes, recirculation regions, and separation flow. This process had no influence on the quality mesh, but the quantity of elements showed a slight increment.

Physics and Boundary Conditions

The physics models selected for this project to simulate the flow field around the different geometries can be divided in two groups, depending on the use of steady or unsteady flow. Both physics models consider the analysis of air in a turbulent flow using the SST turbulence model. For each model, the body surfaces were set as non-slip smooth walls and the contact surfaces as interfaces. The inlet was treated as a velocity inlet and the outlet as a pressure outlet. All other boundaries are far away and they don't disturb the flow around the body, so they were configured as symmetry. Heat transfer was not introduced to minimise the complexity of the simulation. Besides, the rotors were established as rigid blades, in this manner removing any aerodynamic feature arising from blade flapping.

Steady Simulations

These simulations were used to analyse the fuselage and the single rotor models. Steady state simulations were configured to run up to 500 iterations. The mean y+ was of 0.2-0.5 with peak up to 4.5. The computation times were from 6 to 10 hours for the fuselage and from 10 to 12 hours for the rotor, consuming longer time for higher wind speed.

The solutions were calculated following the convergence condition used by FLUENT. This criterion is applied when the residuals values are decreasing on each iteration and they overstep the order of 10-3, at this point the solution is considered accurate enough and the simulation stops. The rotor and full quadrotor steady simulations achieved this convergence after 300 iterations. In the case of the fuselage simulations, the residual values followed a decreasing path, but they didn't surpass the order of 10-3 after 500 iterations. Besides, the monitored values for the Lift coefficient never stabilised and showed an irregular oscillation.

Unsteady Simulations

Unsteady runs are more appropriate to simulate a real world environment. The negative point of unsteady simulations are the resources needed and the high computational times. Unsteady simulations were used for all models and most test cases. Particular importance was given to the analysis of the single rotor and full quadrotor configurations in order to well define the flow interferences and the total thrust variation.

Unsteady simulations were set to complete up to 100 time steps with a maximum of 20 iterations for each time step. The simulations were run during weekends for a maximum of 48 hours limited by the equipment availability. A time step of 0.001 was used to start the simulations, which was increased up to 0.0075 once the simulations were stabilised.

The same convergence condition explained before was applied to the unsteady simulations, but in some cases the residual values decreased fast and there was the risk of the simulation to stop before the flow features were fully developed. For this reason, this condition was cancelled and the residuals values were monitored manually to maintain stable values. The total time simulated was from 0.3 to 0.6 seconds which was enough to fully generate the rotor and the fuselage wakes and the residual values were maintained on the order of 10-3. All simulations showed good convergence, the residual values suffered a constant decrease at the start of the calculations that tended to stabilise as the time steps were solved.

RESULTS

The experimental data obtained from the wind tunnel tests described in section 5 was employed for the validation of the CFD results. The main physical variables measured during the experimental tests were the lift and drag produced by the different parts under diverse flow configurations. Consequently, these were the values compared CFD results in order to determine the quality of the CFD simulations. This validation was carried out in three stages:

- Validation of the fuselage simulations.
- Validation of the rotor simulations.
- Validation of the full quadrotor (fuselage + rotors) simulations.

Validation of the fuselage simulations

The fuselage model was analysed through steady and unsteady simulations. The purpose of the steady simulations was to define the flow features for a general understanding of the physical phenomena occurring around the body. These simulations though, are not expected to produce an accurate definition of the flow. Unsteady simulations were considered for a more realistic solution with the expectation of a good definition of the wake and the separation and recirculation regions.

Steady Simulations

The results, presented in Table 6 and Table 7 show a satisfactory agreement in the drag lectures, which is considered the main value in order to describe the fuselage model. However, the simulations obtained considerably poor results in the lift prediction. Still, the simulations for 5 m/s and 10 m/s velocity inlet obtained lift values with an ascent tendency similar to the wind tunnel tests. On the other hand, the simulations for 15 m/s velocity inlet get lift values quite different to the experimental ones. These discordances might have two main reasons. The first one would be related with the previously mentioned convergence problems undergone during the fuselage simulations, important to point the use of the complex CAD fuselage model on these simulations. The second reason could be related with the concerns regarding the wind tunnel testing and the interferences between the fuselage and the support.

As consequence, the steady simulations for 5 m/s and 10 m/s could be used for a basic understanding of the flow around the body, but could never serve as a precise definition of the flow field. Differently, the simulations for 15 m/s velocity inlet cannot assure a good definition of the problem and were discarded.

Table 4 - CFD results fuselage 0° A.O.A. steady simulations

0° A.O.A	**Lift**	**cfd**	**Drag**	**cfd**
5 m/s	0.14	0.024	0.1	0.08
10 m/s	0.10	0.12	0.35	0.32
15 m/s	-0.04	0.244	0.71	0.77

Table 5 - CFD results fuselage -10° A.O.A. steady simulations

-10° A.O.A	Lift	CFD	Drag	FD
5 m/s	0.10	-0.02	0.12	0.09
10 m/s	0.35	-0.06	0.30	0.34
15 m/s	0.40	-0.31	0.70	0.76

Unsteady Simulations

The values obtained on the unsteady simulations resulted with a better matching on drag lectures, but again with an inconsistent estimation of the lift values as presented in Table 8 and Table 9. Unsteady simulations presented divergence problems as well, but they were solved with the use of a short time step of 0,001 seconds for long part of the simulations to finally obtain well converged solutions. Still, it was considered a divergence problem probably due to the complex geometries involved in this model.

This way, the fuselage simulations were considered appropriated as a guidance to study the generation of drag from the fuselage model. However, the discrepancies found between the test data and the CFD results appear to be of importance enough. Therefore, the fuselage simulations cannot be totally trusted until the cause of these disagreements is clarified through further investigation.

Table 6 - CFD results fuselage 0° A.O.A. unsteady simulations

0° A.O.A	Lift	CFD	Drag	FD
5 m/s	0.14	0.04	0.1	0.09
10 m/s	0.10	0.12	0.35	0.34
15 m/s	-0.04	0.32	0.70	0.72

Table 7 - CFD results fuselage -10° A.O.A. unsteady simulations

-10° A.O.A	Lift	CFD	Drag	CFD
5 m/s	0.10	0.01	0.12	0.10
10 m/s	0.35	-0.20	0.30	0.30
15 m/s	0.40	-0.32	0.70	0.70

Validation of the rotor simulations

The circular movement of the rotors made necessary the implementation of moving reference frames in the rotor model. As explained in section 4.4, two of the methods applicable to the present problem are multiple reference frame (MRF) model and Sliding mesh model, related with steady and unsteady simulations respectively. The objective of this section is to determinate whether or not these methods are valid to our problem for the different test cases.

Steady Simulations

The steady simulations of the rotor were only likely to produce good results on hover flight as this is the only case that can be considered as a steady state problem and therefore fully applicable to the MRF model. As expected, the results on Table 10 and Table 11 present a good prediction of the hover flight condition, but unreliable values for the rest of the cases. The discrepancies are especially noticeable in the values obtained for the rotor at -10° of angle of attack. Where the experimental data shows stable lift for all wind tunnel speeds, while the CFD simulations predict a constant increase for the same values. This probes that the MRF model is missing certain aerodynamic effects acting on the rotor flow field. The reason for this, is the highly unsteady flow generated by the interaction between the flows from the rotor circular movement and the incoming wind, impossible to be captured through this method.

Table 8 - CFD results rotor 0° A.O.A. steady simulations

0° A.O.A	Lift	CFD	Drag	CFD
0 m/s	0.24	0.26	0.00	0.00
5 m/s	0.24	0.33	0.04	-0.01
10 m/s	0.31	0.48	0.04	0.00
15 m/s	0.33	0.48	0.10	0.00

Table 9 - CFD results rotor -10° A.O.A. steady simulations

-10° A.O.A	Lift	CFD	Drag	CFD
0 m/s	0.24	0.26	0.00	0.00
5 m/s	0.25	0.26	0.00	-0.01
10 m/s	0.23	0.38	0.05	-0.02
15 m/s	0.25	0.76	0.06	-0.03

Unsteady Simulations

The sliding mesh model is a much more powerful method, designed to fully describe the real world physical phenomena arising from rotating bodies. In fact, the unsteady simulations for the rotor model achieved reasonably good results when comparing to the experimental data. Looking at Table 12 and Table 13 we can detect a good agreement between the values. Nonetheless, small discrepancies are also present, these are discussed next. In first place, is it visible how the predicted lift values show an over-prediction in most simulations. This disagreement though, was not considered as a wrong result, given that the fuselage-rotor interference could have produced that decrease on the lift during the wind tunnel tests.

Secondly, it can be appreciated a small inconsistency on the drag values for the rotor at 0° of angle of attack. In this case the unlike values might be due to the differences between the real model and the CAD model used on the simulations, like the variations introduced on the central part of the rotor and the lack of high on the original CAD design. This last reason would also explain the good matching on the drag lectures for the rotor at -10° of angle of attack, as the wind would impact the blade before the hub, generating a lower direct interference with this configuration.

Having in count the previous explanations, the sliding mesh model can be considered a solid method for the prediction of the aerodynamic features arising from the propeller for the present project.

Table 10 - CFD results rotor 0° A.O.A. unsteady simulations

0° A.O.A	Lift	CFD	Drag	CFD
0 m/s	0.24	X	0.00	X
5 m/s	0.24	0.35	0.04	0.04
10 m/s	0.31	0.36	0.04	-0.01
15 m/s	0.33	0.40	0.10	0.01

Table 11 - CFD results rotor -10° A.O.A. unsteady simulations

-10° A.O.A	**Lift**	**CFD**	**Drag**	**CFD**
0 m/s	0.24	X	0.00	X
5 m/s	0.25	0.28	0.00	0.00
10 m/s	0.23	0.32	0.05	0.05
15 m/s	0.25	0.36	0.06	0.09

Validation of the full quadrotor simulations

The full quadrotor simulations were introduced to predict the flow physics involving the quadrotor under the different flow configurations in order to obtain an accurate description of the flow field. The previous section proved that the MRF model was not suitable for the quadrotor problem and for this reason, only unsteady simulations with the sliding mesh model were considered for the full quadrotor model.

As presented in Table 14 and Table 15 the quadrotor unsteady simulations achieved decent results matching with the test data. The predicted values were close to the experimental ones and they followed the same changing tendency, which is an increase on lift and drag as the wind tunnel speed increases. As a negative point, the lift predictions showed an assumable but persistent under-prediction, which might be due to the rigid blade assumption. Something similar happened to the drag estimations for 15 m/s velocity inlet; this occurrence seems due to the use of the simple fuselage CAD model, not so representative of the original one. Overall though, it can be said that the full quadrotor simulations presented optimistic results with good agreement with the test data.

The quadrotor flight simulations involve complex flows and need of further analysis, especially for the aerodynamic features arising from the fuselage-rotors interaction. The next section covers a more detailed analysis of this model with the intention to offer a better description of the quadrotor flow field under the different flow configurations.

Table 12 - CFD results full quadrotor 0° A.O.A. unsteady simulations

0° A.O.A	**Lift**	**CFD**	**Drag**	**CFD**
0 m/s	0.96	0.80	0.00	0.00
5 m/s	1.12	0.86	0.25	0.26
10 m/s	1.3	1.13	0.5	0.50
15 m/s	1.75	1.76	1.14	0.95

Table 13 - CFD results full quadrotor -10° A.O.A. unsteady simulations

-10° A.O.A	**Lift**	**CFD**	**Drag**	**CFD**
0 m/s	0.93	X	0.00	X
5 m/s	1.21	0.92	0.25	0.30
10 m/s	1.42	1.22	0.51	0.46
15 m/s	1.79	1.64	0.95	0.72

Flow Analysis

Due to the complexity of the unsteady flow around the full quadrotor model, the comparison of the results and their analysis is not a simple task. On this section, we proceed then to the flow analysis, going from the examination of the velocity and pressure contours to the investigation of the main features of the flow field in local regions. The stating point will be a quick analysis of the fuselage and single rotor simulations to finish with a more detailed examination of the full quadrotor simulations.

Fuselage

This analysis presents a good opportunity to visualise the changes on the pressure and velocity distributions between the fuselage simulations and the full quadrotor simulations, in order to clarify the impact of the revolving rotors. For a not too extensive analysis of the fuselage, only the contours of the simulations for 10 m/s velocity inlet were considered for this analysis. These simulations are expected to serve as a general case to describe the aerodynamics occurring on the fuselage flow field.

Starting with the simulations for 0° of angle of attack, the velocity contour and the vector velocity field of the symmetry plane on Fig. 27 and Fig. 28 constitute an overview of the velocity distributions around the fuselage. The blue areas indicate a velocity drop happening in those regions. The velocity drop on the front seems to be due to the collision between the air and the body surface. The low velocities on top, bottom and back are attributed to separation flow with recirculation regions which are the main contribution to the drag force. This separation is especially large on the bottom due to the sharp edge. The top and bottom separation continue along the fuselage and joint to the wake generated at the back, which presents two small counter rotating recirculation areas on the central back of the body. The resultant wake seems to start to vanish after the body and then recovers strength to finally disappear. The second part of the wake might be due to the separation flow generated by other parts of the body like the legs or the edges as presented in Fig. 29. Also noticeable two high speed regions on top and bottom just out of the separation bubbles.

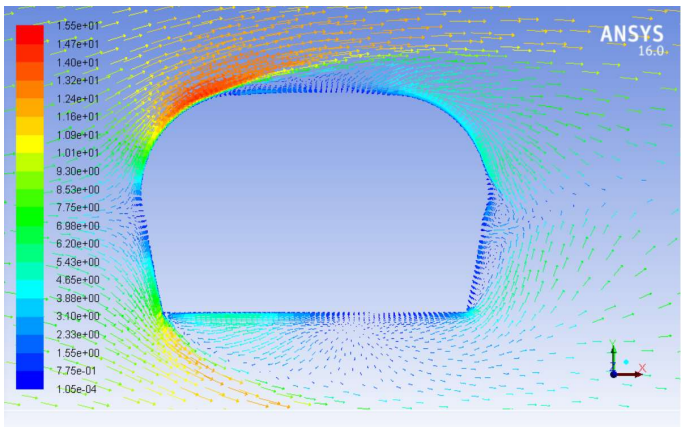

Figure 5: Velocity vectors fuselage model at 0° A.O.A for the symmetry plane

The pressure distribution can be appreciated on Fig. 30 and Fig. 31. They show an elevated pressure gradient around the fuselage,

which means that the majority of the drag is due to the pressure force. The highest pressure values are found on the front of the body indicating a stagnation area. After that, we can find negative pressure values due to the separation flows. The lowest pressure values are located on the top front. The top also presents a larger area of negative pressure, which may explain the positive lift generated by the fuselage under this flow configuration.

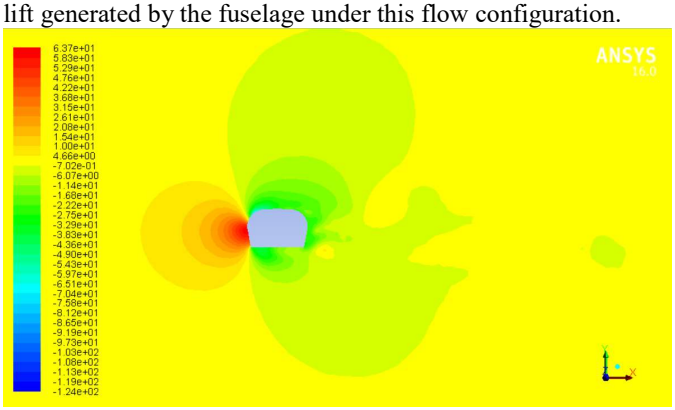

Figure 6: Pressure contour fuselage model at 0° A.O.A for the symmetry plane

The simulation for the fuselage at -10° of angle of attack presented the similar features, but there are important changes on the velocity and pressure distributions. The velocity drop on the front happens in similar manner, but with a smaller area of effect. Looking at figure 7, separation flows can be found on the top, bottom and back of the body. The introduction of a negative angle of attack reduces the top separation flow, which reattaches to the body surfaces before the wake starts. The bottom separation, much larger than the top one, joins the back wake that develops a large recirculation region behind the body.

Rotor analysis

The analysis of the rotor simulations intends to clarify the changes of the lift generated under the different flow configurations. According to literature and to the wind tunnel tests, the effect of the transitional lift increases with higher incoming wind speed and the decrease of the angle of attack of the propeller produces a lower lift generated.

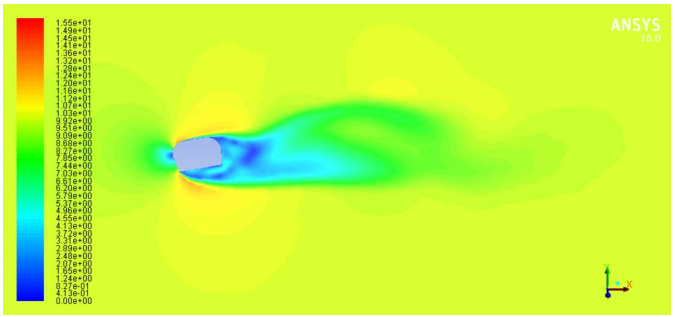

Figure 7:Velocity contour fuselage model at -10° A.O.A for the symmetry plane

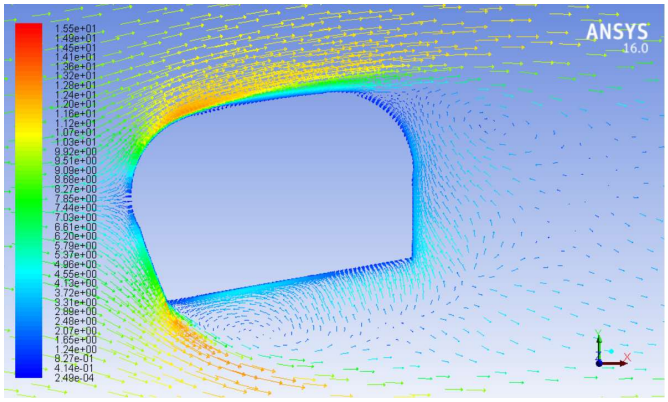

Figure 8:Velocity vectors fuselage model at -10° A.O.A for the symmetry plane

For a better understanding of the transitional lift effect, we can consider first the hovering and the forward flight simulations. In Figure 9, we can find the velocity vectors on the middle plane around the rotor for 0 m/s and 5 m/s velocity inlet. The wind impacts the rotor in different directions that can be discomposed in a negative y and a positive x component. Usually, the transitional lift is studied on forward flight where the incoming wind creates a more elevated horizontal component as the vehicle moves faster. This increase on the horizontal component induces a decrease on the vertical component opposite to the rotor and therefore an increase on lift.

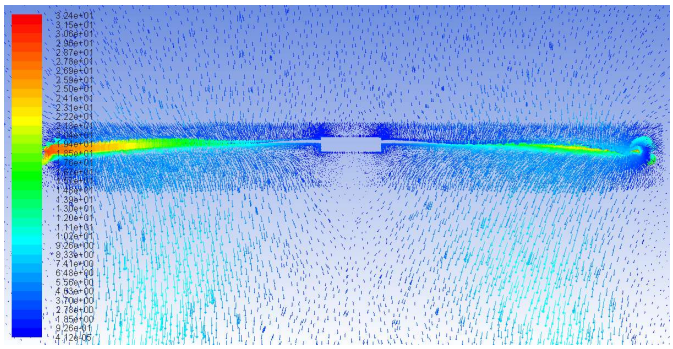

Figure 9: Velocity vectors rotor model hover flight

Full Quadrotor analysis

The analysis of the full quadrotor simulations involves the described physical phenomena produced by the fuselage and rotors with the addition of the rotor-fuselage interference. The objective of this section is to interpret the CFD results in order to understand the behaviour of the quadrotor flow field. For this purpose, the simulations for 0° of angle of attack were considered, as they presented representative results.

A hovering rotor may be considered as a quasi-steady problem, but the introduction of the fuselage converts this to a fully turbulent flow. Figure 10 presents the velocity contour of the rotors plane; on which the symmetrical wakes seem to be distorted by the fuselage. Also to point a drop of velocity between the rotors, probably due to the existence of vorticity on that location.

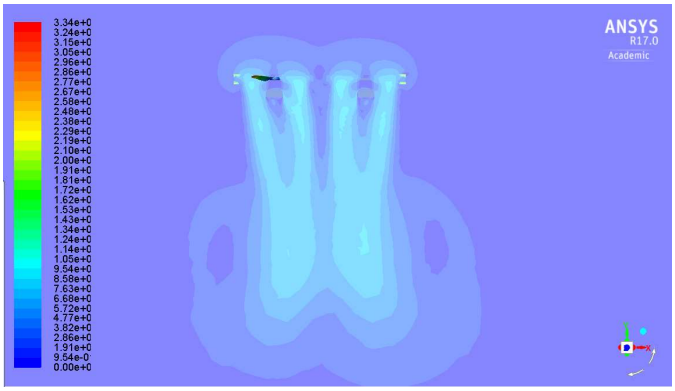

Figure 10 Velocity contour hover flight

In Figure 10 we can see how the rotors suck air from the top, sides and the space between them. It is in this location where ascending flows join with descending flows creating two counter rotating recirculation areas. There are two important velocity drop areas between the fuselage and the rotors and bellow the fuselage, with strong recirculation in the last one, creating lift,

CONCLUSIOS

In this study, the quadrotor flow field and the aerodynamic forces created by the different parts were analysed through CFD techniques. A theoretical approach was presented to serve as basis for the rest of the project. An experimental wind tunnel testing was carried out and the data were used for the validation of the CFD simulations. The quadrotor parts were designed in CAD tools and exported to ANSYS meshing to create three models, a full quadrotor configuration and two stripped versions for the fuselage and a single rotor. Unstructured meshing was used and rotatory cell zones were introduced to allow the simulation of the rotors movement.

Steady and unsteady flow simulations with a SST turbulence model are used. Hover and forward and side wind cases were inspected. Hover case was examined with 0° of angle of attack, side case with 0° of angle of attack for 5 m/s, 10 m/s and 15 m/s regarding the free stream velocity incident on the rotors. Similar for the forward case, but with -10° of angle of attack.

A validation of the CFD results was carried out, comparing Lift and Drag values with the experimental results. Steady simulations showed inconsistent agreement in many cases and were incapable of capturing some of the most important aerodynamic effects, such as transitional lift. Unsteady simulation achieved an overall good match with the experimental data. Only the lift values for the fuselage model at 10° of angle of attack were different, however, this discrepancy was attributed to the aerodynamic interference between the fuselage and the support used in the wind tunnel testing. t has also introduced some of the causes of stability problems and defined the main causes of lift and drag for the different models. From these results, a decent prediction of the flow can be expected. The simulations were considered reliable enough to analyse the flow and point out the main aerodynamic features with conviction.

Overall, this study has demonstrated that CFD simulations can perfectly describe complex flows with rotatory movement especially quadrotor flow that is of high demand practically. I

REFERENCES

[1] Hoffmann, G. M., Waslander, S. L., and Tomlin, C. J. (2006) Distributed Cooperative Search using Information-Theoretic Costs for Particle Filters with Quadrotor Applications. *Proceedings of the AIAA Guidance, Navigation, and Control Conference.* Colorado, United States of America, 21-24 August 2006.

[2] Leishman, J.G. (2006) *Principles of Helicopter Aerodynamics*. 2nd ed. New York: Cambridge University Press.

[3] Seddon, J. and Newman, S. (2011) *Basic helicopter aerodynamics*. 3rd ed. West Sussex (UK): John Wiley and Sons.

[4] Hoffmann, G. M., Waslander, S. L., and Tomlin, C. J. (2009) Aerodynamics and Control of Autonomous Quadrotor Helicopters in Aggressive Maneuvering. *Proceeding of the IEEE international conference on Robotics and Automation.* Kobe (Japan) 12-17 May 2009.

[5] Anderson, Jr, J.D. (1995) *Computational Fluid Dynamics: the basics with applications*. New York: McGraw-Hill.

[6] Versteeg, H.K. and Malalasekera, W. (1995) *Computational Fluid Dynamics: The Finite Volume Method*. Essex, England: Longman Scientific & Technical.

[7] Batchelor, G.K. (2000) *An INTRODUCTION to FLUID DYNAMICS*. 3rd ed. Cambridge: Cambridge University Press.

[8] Ruban, A.I. and Gajjar, J.S.B. (2014) *Fundamentals of Fluid Dynamics. In: Fluid Dynamics: Part 1: Classical Fluid Dynamics*. Oxford University Press.

[9] Tennekes, H. and Lumley, J.L. (1972) *A First Course in Turbulence*. United States of America: Mit Press.

[10] Tu, Y., Yeoh, G. and Liu, C. (2013) *Computational Fluid Dynamics: A Practical Approach*. 2nd ed. Oxford, Uk: Butterworth-heinemann.

[11] Kapadia, S. and Roy, S. (2003) Detached eddy simulation over a reference Ahmed car model. *American Institute of Aeronautics and Astronautics*.

[13] Merzari, E. and HinokataSandberg, H. (2009) Development of an LES Methodology for Complex Geometries. *Nuclear Engineering and Technology*. 41 (7)

[14] Umale, S. and Khan, R.S. (2004) Cfd aerodynamic analysis of the Ahmed body. *International Journal of Engineering Trends and Technology*. 18 (7)

[15] Furbo, E. (2010) *Evaluation of RANS turbulence models for flow problems with significant impact of boundary layers.* Uppsala Universitet.

[16]Pope, S.B. (2000) *Turbulent Flows*. Cambridge: Cambridge University Press.

[17] Steijl, R. and Barakos, G., Sliding mesh algorithm for CFD analysis of helicopter rotor–fuselage aerodynamics, Int. J. Numer. Meth. Fluids 2008; 58:527–549.

[18] Marcel I. Numerical study of helicopter blade-vortex mechanism of interaction using large-eddy simulation. Comput Struct, 2009, 87: 758–768

[19] Massimo G, Giovanni B. Novel boundary integral formulation for blade-vortex interaction aerodynamics of helicopter rotors. AIAA J, 2007, 45: 1169–1176

[20] Steijl R, Barakos G N. Computational study of helicopter rotorfuselage aerodynamic interactions. AIAA J, 2009, 47: 2143–2157

[21] Xu H Y, Ye Z Y. Numerical simulation of rotor-airframe aerodynamic interaction based on unstructured dynamic overset grids. Sci China Tech Sci, 2012, 55: 2798–2807